Research Square

Preprints are preliminary reports that have not undergone peer review.
They should not be considered conclusive, used to inform clinical practice,
or referenced by the media as validated information.

Thermo-Mechanical Modelling of Residual Stress and Warpage in Additively Manufactured CF-PEKK

Awe Victoria Damilola

awevictoriadamilola@gmail.com

Jomo Kenyatta University of Agriculture and Technology

Rehema Ndeda[1]

Jomo Kenyatta University of Agriculture and Technology

Kabini Karanja

Jomo Kenyatta University of Agriculture and Technology

Tshenolo Leso[2]

Botswana International University of Science and Technology

Research Article

Keywords: Fused Filament Fabrication, Additive Manufacturing, CF-PEKK, Lightweighting

Posted Date: November 26th, 2026

DOI: https://doi.org/10.21203/rs.3.rs-11728404/v1

License: This work is licensed under a Creative Commons Attribution 4.0 International License.
Read Full License

Thermo-Mechanical Modelling of Residual Stress and Warpage in Additively Manufactured CF-PEKK

Awe Damilola Victoria[1*], Rehema Ndeda[1], Kabini Karanja[1], Tshenolo Leso[2]

[1]Department of Mechatronic Engineering, Jomo Kenyatta University of Agriculture and Technology, Nairobi, Kenya

[2]Department of Chemical, Materials & Metallurgical Engineering, Botswana International University of Science and Technology, Palapye, Botswana

[*]Corresponding author (Email: awe.victoria@students.jkuat.ac.ke , ORCID: 0009-0005-5248-5286)

Abstract

The demand for lightweight materials in electric vehicles (EVs) has spurred research into high-performance composites. Additive manufacturing (AM) has also gained popularity for the production of composites due to the ability to produce complex and lightweight structures. The uptake of high-performance composites such as carbon fiber-reinforced polyetherketoneketone (CF-PEKK) has, however, been slowed by the limited information on the behavior of CF-PEKK when additively manufactured. This study aims to investigate the behavior of CF-PEKK and aluminium under structural loading conditions and simulate CF-PEKK's thermal response during Fused Filament Fabrication (FFF) printing. A numerical modelling platform using multiscale modelling that combined the DIGIMAT micromechanics model and ANSYS FEA was developed to predict the tensile strength, residual stress, and warpage. The predicted maximum stress of CFPEKK is 118.99 MPa, compared to that of aluminium of 117.73 MPa. The Taguchi L9 design of experiments was used to evaluate the effects of process parameters on residual stress and warpage. The optimum parameter combination was found to be 0.25 mm for the layer thickness, 430 °C for extrusion temperature, 160 °C for chamber temperature, and 40 mm/s for the printing speed.

Keywords: Fused Filament Fabrication, Additive Manufacturing, CF-PEKK, Lightweighting, DIGIMAT-AM

1.0 Introduction

The transportation and automotive industry today is faced with a major challenge in the form of the need for higher energy efficiency, driven by ever-increasing stringent emissions standards and the need to reduce greenhouse gas emissions, as the transportation sector still accounts for a sizable portion of the global carbon emissions [1]. Weight reduction is one approach currently used to enhance energy efficiency. In electric mobility, lightweight structural components increase battery range and improve handling, while retaining structural integrity and performance [2]. In electric motorbikes, the motor housing serves three key purposes: encloses the motor, provides mechanical attachment to the vehicle body, and heat dissipation while in use. The motor housing material is, therefore, required to possess high stiffness, durability and good heat dissipation [3]. However,

most motor housings that possess these properties are also heavy due to the prominent use of metals.

Metals are often preferred for the manufacture of components that require high strength and toughness. Steels are widely used in the production of EV parts because of their machinability and high tensile strength [4]. The use of aluminium alloys has also been widespread in the manufacture of electric vehicle components because of their good heat conductivity and machinability [5]. The two aluminium alloys commonly used in the production of e-bike parts include AA 6061 with Mg and Si as major alloy constituents and AA7005 with Zn as the major alloy constituent [6]. However, the inherent density of metals limits any further weight reduction.

High-performance composite materials have recently been introduced in electric vehicles due to their high strength and stiffness, which makes them a viable alternative to metals. The density of these composites is often lower than that of metals, which makes it a suitable lightweight alternative [7]. Fiber-reinforced motor housings have been adopted in the automotive industry due to their corrosion resistance and lower weight [8]. Carbon fiber reinforced polymer (CFRP) was used to reduce the weight of material for an electric motor casing by Boopathi et al. [9]. The outer casing material of the motor was changed from aluminium to Carbon fiber reinforced polymer, resulting in a 20.27 % reduction in weight.

Carbon Fiber Reinforced Polyetherketoneketone (CF-PEKK) is 45–50% lighter than aluminium due to its density of 1.0–1.39 g/cm^3 [10]. Its fatigue behaviour is outstanding, with excellent super corrosion resistance. These characteristics make CF-PEKK suitable for long-term durability in automotive applications [11]. However, CF-PEKK has low thermal conductivity at 5 and 20 W/m·K compared to Aluminium. The performance of CF-PEKK depends on its configuration. Laminates and short design configurations of CF-PEKK have higher longitudinal, tensile and shear strength as a result of improved fiber-matrix interfacial adhesion and proper consolidation between deposited layers during melting [12, 13, 14].

Fused Filament Fabrication (FFF) is promising for manufacturing lightweight structures and producing complex geometries for CFRP parts [15, 16]. Rinaldi et al. [67] showed that the FDM-printed PEEK can meet the strict requirements of both mechanical and thermal performance for space structures. They demonstrate that PAEK-based materials may be lightweight substitutes for metallic structures in the case of special engineering applications. Han et al. [68] studied warpage in material extrusion of PEEK by thermal simulations and showed that elevated processing temperatures and thermal gradients lead to residual stresses causing dimensional inaccuracies and geometric distortion in printed parts. Sun et al. [51] developed a theoretical model to predict warpage of carbon-fibre-reinforced PEEK composites fabricated by FDM. Their results showed that the thermal gradients induced by processing generate residual stresses that result in dimensional distortion. Carbon fiber reinforcement reduces the warpage due to its high thermal conductivity and low Poisson's ratio.

One of the main challenges of FFF of carbon fiber reinforced polymers is that they exhibit microstructural alterations during material deposition, leading to matrix degradation and anisotropic mechanical behaviour [17]. Zhang et al. [25] established that the matrix of CF/PEKK showed strong temperature dependence, with the elastic modulus decreasing as temperature increased. The interfacial bonding properties of the composite deteriorated progressively as temperature increased. Belei et al. [21] observed defects in a polyamide matrix reinforced with short carbon fibers during FFF printing of tensile specimens. The specimens were observed to contain carbon sputters. It was deduced that during FFF, short fibers exhibit increased anisotropy in the orientation of deposition depending on the stacking sequence of the layers. Hu et al. [18] also investigated the effect of processing stages on the damage caused to continuous carbon fibers during different stages of the Fused Deposition Modelling (FDM) process. Most damage occurred at the final stage when the FDM filament was bent through 90° and pressed onto the build platform, causing broken and damaged fibers in the filament.

Warpage is another defect typically observed during FFF. Al-Dhaheri et al. [20] investigated the effect of processing conditions on warpage in CF/PEKK using a multilevel Design of Experiments, while the effect of the factors on warpage was established through Analysis of Variance. The major factors contributing to warpage are the number of layers and consolidation pressure. By using layered panels with a variation in layer thickness and the associated deposition configurations, warpage was significantly reduced, especially with alternating raster angles (±45°) between successive layers for balancing residual stresses [39].

Alramsi [19] studied the effect of warpage of CF-PEKK and PEEK in AFP printing. Warpage was increased when the pressure was lowered below 2 bar in Automated Fiber Placement (AFP). Warpage was reduced at optimum process parameters, that is, pressure at 4 bar, frequency at 67 Hz, and a hot-plate substrate as the base for layer tapering. This reduced the thermal stresses, which enhanced laminate quality.

Residual stress has also been observed in FFF-printed CFRP composites. Print orientation of CF-PEKK tensile specimen was observed as key factor in residual stress by Rashed et al. [22] who noted increased residual stress in samples printed in a horizontal position on the build plate, particularly in the lower layers where thermal gradients are most pronounced. This concentration of stress resulted in swift plastic deformation owing to localized delamination of raster layers adjacent to the build plate interface. The specimen's residual stress was reduced by printing the samples edge-on rather than flat on the build plate. According to Enriconi et al. [26], residual stresses for FFF-printed specimens arise post-deposition, that is, during cooling and solidification. Phase transitions and thermal dissipation at this stage increase residual stresses. The impact of process parameters on temperature effects has also been investigated. Maloney et al. [23] observed the impact of printing speed and platform temperature on residual stress during FFF printing of CF-PEKK specimens. An increase in the residual stress was observed as the printing speed

increased, while an increased build platform temperature improved adhesion to the build platform, thereby reducing residual stress and improving interlayer bonding. Optimization of the printing parameters could positively impact post-deposition effects.

The effect of important FFF process parameters like layer thickness, raster orientation, and thermal profiles on the structural and mechanical properties of 3D printed PEEK and PEI parts was studied by El Magri et al. [66], who showed that the selection of parameters is critical to interlayer adhesion, degree of crystallinity, and the subsequent anisotropic mechanical response of high-performance polymer components. The selection of the fused filament fabrication (FFF) process parameters was guided by findings from previous experimental investigations of polyaryletherketone (PAEK)-based materials and fiber-reinforced thermoplastic composites. The mechanical performance of FFF-processed materials is influenced by material properties, thermal history, interlayer adhesion, porosity, fiber alignment, and crystallinity [64]. Previous studies have also identified nozzle temperature, layer thickness and build orientation as important factors affecting the microstructure and mechanical properties of additively manufactured PEKK components [22, 55].

Nozzle temperature influences the polymer melt viscosity and the conditions governing interlayer diffusion and bonding. Triminì et al. [61] investigated the effects of nozzle temperature, chamber temperature and printing speed on the crystallinity and tensile properties of PEEK. Their results are further evidence for the importance of controlling the thermal conditions during the processing of semi-crystalline PAEK polymers. The temperature of the chamber is of special importance for high-performance thermoplastics, since it determines the temperature difference between the deposited material and its environment. A Taguchi-based investigation of PEEK and PEKK identified chamber temperature as an important factor affecting PEKK yield strength, while layer height and printing speed influenced stiffness. The study also reported an influence of processing temperatures on material crystallinity [62]. In addition, differences between nozzle, layer thickness, and chamber temperatures have been associated with residual stress development during PEKK processing [32, 59].

Printing speed was included because of its influence on material deposition and thermal history. Besides layer thickness, nozzle temperature and build-platform temperature, Maloney et al. [23] investigated the printing speed and its effects on crystallinity, porosity and flexural properties in semi-crystalline PEKK. Triminì et al. [61] also studied the printing speed as a function of nozzle and chamber temperatures, while Tetteh et al. [56] investigated its effect on the mechanical response of PAEK materials processed by FFF.

Layer thickness was selected because it affects the number of deposited layers, interlayer contact, thermal history and surface characteristics of FFF components. Hu et al. [18] identified layer height as an influential factor affecting the flexural strength of CFR-PEKK and reported an experimentally investigated optimum of 0.25 mm. Maloney et al. [23] also examined layer

thickness in PEKK and reported an optimum of 0.1 mm under their investigated conditions. Further evidence of its relevance is provided by a study of CF-PEEK in which specimens were produced at layer thicknesses of 0.1 and 0.2 mm to investigate their mechanical and surface characteristics [63].

The Taguchi L9 orthogonal array has been employed to optimize the process parameters for minimum residual stress and warpage. One of the factors reported to affect the quality and mechanical properties of high-temperature materials during FFF is nozzle temperature. Hu et al. [18], through experimental studies, considered nozzle temperature along with layer height, print speed, raster angle, and nozzle diameter using the Taguchi method. The study investigated variation of parameters such as nozzle diameter, layer height, printing speed, raster angle, and nozzle temperature. It was observed that raster angle and layer height had the most influence on the flexural strength of CFR-PEKK. The optimum parameters obtained were raster angle of 0/90°, layer height of 0.25 mm, a nozzle diameter of 0.8 mm, nozzle temperature of 375 °C, and print speed of 1100 mm/min. These parameters simultaneously influence the flexural properties of printed CFR-PEKK. Maloney et al. [23] optimised FFF process parameters for unreinforced PEKK and found that a combination of high nozzle temperature (380 °C), low print speed (30 mm/s), thin layers (0.1 mm), and elevated plate temperature (140 °C) minimised void formation, enhanced crystallinity, and yielded flexural properties approaching 80% of injection-moulded equivalents.

Thermomechanical simulation has been used to understand the properties and behaviour of the materials during processing. They provide suitable numerical estimations of the effect of temperature on the properties, deformation, and failure mechanisms of composite materials, thus allowing better understanding of the correlation between material microstructure and its performance and use it for optimization purposes without conducting expensive experiments [24]. Thermomechanical modelling is useful in the prediction of the behaviour of the material during the additive manufacturing process. There have also been limited attempts made towards developing modelling techniques and experimental verification with respect to minimizing warping as well as enhancing the performance of CF-PEKK tensile specimens produced through FFF processes. Significant attention has been paid to the investigation of properties of fiber-matrix interaction, interlayer adhesion, and cooling process of CF-PEKK produced using FFF technology. However, limited studies have focused on the impact of FFF printing variables (printing speed, thickness of layers, and the temperatures of both the chamber and nozzle) on post-deposition effects such as warpage and residual stress. For CF-PEKK, there is little evidence available on the influence of process variables on warpage and residual stress. In this study, a thermo-mechanical model was developed to predict the effects of warpage and residual stress during FFF of CF-PEKK for a motor housing of an electric motorbike [27].

2.0 Materials and Methods

2.1 Material Properties

In this study, we compared the mechanical performance of CF-PEKK with a conventional lightweight engineering material, aluminium. The CF-PEKK material was selected for its high-performance thermoplastic matrix and carbon-fiber reinforcement, which could provide potential benefits for lightweight structural applications related to electric mobility. Aluminium was included as a reference material for comparative structural assessment.

The material properties used in the numerical analyses are presented in Table 1. According to the aluminium material datasheet reported in [45], aluminium has a melting temperature of 660.37 °C and a density of 2.6989 g/cm³. The CF-PEKK material, obtained from the 3DXTECH datasheet [28], has a glass transition temperature of 143 °C, an approximate melting temperature of 305 °C and a density of 1.39 g/cm³. The reported mechanical and thermal properties were used as the input material data for the respective numerical models.

Table 1. Material properties of CF-PEKK and aluminium

Property	CF-PEKK	Aluminium
Tensile modulus (MPa)	8100	68000
Glass transition temperature (°C)	143	–
Tensile strength (MPa)	105	90–100
Flexural strength (MPa)	136	–
Flexural modulus (MPa)	8300	68000
Melting temperature (°C)	305	660.37
Density (g/cm³)	1.39	2.6989
Heat deflection temperature (°C)	265	–

2.2 CAD Modelling and Structural Finite Element Analysis

The tensile specimen was developed as a 3D model in a computer-aided design (CAD) system using Autodesk Inventor based on the tensile testing standard ASTM D638 [34]. The geometry of the specimen was exported to ANSYS Workbench 2024 R1 for finite element analysis (FEA). CAD representation of the tensile specimen is shown in Fig. 1.



Figure 1: CAD View of Tensile Specimen

Finite element analysis was performed separately on the CF-PEKK and aluminium specimens to compare the mechanical response of the structure under an imposed tensile load. The simulations were performed using the ANSYS Workbench platform [31] and the material properties are given in Table 1. A fixed-support boundary condition was applied at one end of the specimen, and a tensile force was applied at the other end. The stress distribution and deformation response of both materials were assessed under the prescribed structural loading conditions in this loading configuration. Figure 2(a) and (b) show the boundary conditions applied to the specimens, which are the fixed support and the applied tensile load, respectively.

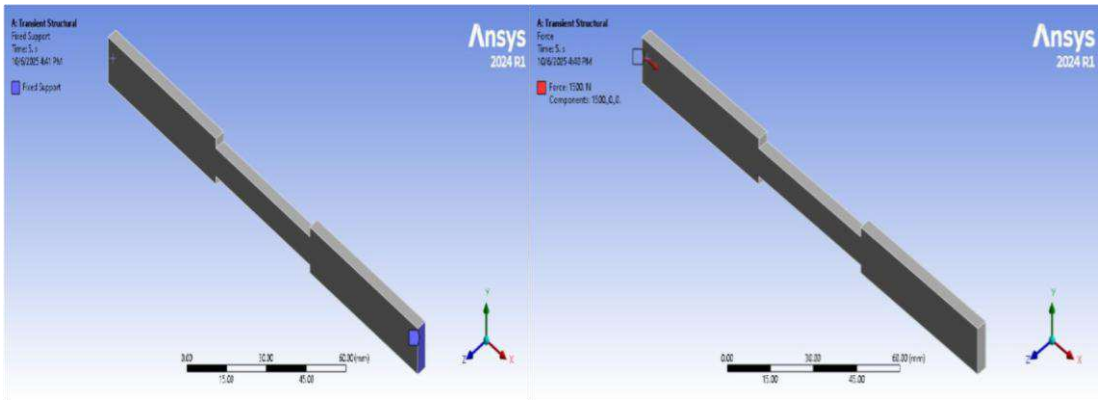

Figure 2: Boundary conditions applied to the specimen (a) Fixed support at one end (b) Applied load at the other end

A mesh sensitivity study was carried out to assess the effect of element size on the predicted stress response. To assess the sensitivity of the numerical predictions to mesh refinement, the stress distributions of mesh sizes 0.7 mm and 4.3 mm were compared.

The material properties of the carbon-fibre-reinforced polyetherketoneketone (CF-PEKK) composite were defined based on the manufacturer's technical datasheet and relevant published literature to model the mechanical behavior [28]. The composite was represented as an equivalent

homogeneous orthotropic material in both ANSYS and DIGIMAT AM to account for its direction-dependent mechanical behaviour arising from fibre reinforcement. The individual carbon fibres and polymer matrix were not explicitly resolved at the microscale.

This equivalent material representation provided a computationally efficient approach for investigating the thermomechanical response of CF-PEKK, particularly residual stress development and warpage, while maintaining a consistent orthotropic material description across the two simulation frameworks.

2.4 Thermo-Mechanical Governing Equations

The thermal and structural behaviour of the CF-PEKK material was investigated based on well-established principles of heat transfer and continuum mechanics. The thermal analysis was carried out in DIGIMAT using the transient heat conduction formulation, which describes the evolution of temperature in a material as a function of time, thermal conductivity, specific heat capacity and internal heat generation [69]. The structural response was then analyzed by ANSYS under mechanical loading with transient structural analysis. The formulation was based on the principles of dynamic equilibrium and linear elasticity. The CF-PEKK material was modelled as an isotropic homogeneous linear elastic solid [30, 70]. The transient heat transfer process can be represented by the energy conservation equation:

$$\rho Cp \left(\frac{\partial T}{\partial t}\right) = \nabla.(k\nabla T) + Q \qquad Eqn\ (1)$$

where ρ is the material density (kg/m³), Cp is the specific heat capacity (J/kg·K), T is temperature (K), t is time (s), k is thermal conductivity (W/m·K), and Q represents the volumetric heat generation rate (W/m³). The structural response under mechanical loading is governed by the dynamic equilibrium equation:

$$\nabla . \sigma + f = \rho \left(\frac{\partial^2 u}{\partial t^2}\right) \qquad Eqn\ (2)$$

where σ is the stress tensor (Pa), f is the body-force vector per unit volume (N/m³), ρ is the material density (kg/m³), u is the displacement vector (m), and t is time (s).

For an isotropic linear elastic material, the stress–strain relationship is expressed using Hooke's law:

$$\sigma = 2\mu\varepsilon + \lambda\, tr(\varepsilon) I \qquad Eqn\ (3)$$

where:

σ is the stress tensor (Pa), μ is the shear modulus (Pa), λ is Lamé's first parameter (Pa), ε is the strain tensor, tr(ε) is the trace of the strain tensor, and I is the second-order identity tensor.

The elastic constants are related to Young's modulus (E) and Poisson's ratio (ν) as shown in Equation 4 and 5 respectively

$$\mu = E\ /[2(1+\upsilon)] \qquad Eqn\ (4)$$

$$\lambda = E\upsilon\ /[(1+\upsilon)(1-2\upsilon)] \qquad Eqn\ (5)$$

For this study, the DIGIMAT-AM deposition-process simulation was conducted with uniform material properties throughout. Thus, the material-property representation used did not explicitly include temperature-dependent changes of the given material properties. The thermal and mechanical response obtained thereby was evaluated using the defined constant material property inputs. The predicted residual stress distribution and displacement field were then utilized to study the internal stress state and dimensional distortion of the simulated component.

2.5 Process Simulation and Numerical Analysis

The Fused Filament Fabrication (FFF) process was simulated with DIGIMAT-AM 2024 to study the effect of the manufacturing conditions on the thermo-mechanical response of CF-PEKK. The simulation modelled the deposition of the material in layers and provided the thermal history during printing and subsequent cooling. The predicted thermal history was used in the process simulation to evaluate the development of residual stresses and the associated dimensional changes.

The manufacturing parameters considered in the simulation were extrusion temperature, chamber temperature, printing speed, and layer thickness. These parameters were investigated to determine their effect on the predicted thermo-mechanical response of the printed component.

The simulation was also used to assess the residual stress distribution and warpage resulting from the deposition and cooling process. The residual stress was obtained from the stress distribution in the simulated geometry. The warpage was evaluated from the displacement field in relation to the original build's geometry. The magnitudes of the resulting displacements indicated the dimensional distortion associated with the build-up of process-induced stresses.

The first reported simulation was performed based on the selected process parameters, which were an extrusion temperature of 430 °C, a printing speed of 40 mm/s, a layer thickness of 0.15 mm, and a chamber temperature of 120 °C have been chosen from the optimum ranges reported in literature for CF-PEKK/PEKK additive manufacturing, so as to reproduce realistic processing conditions in the computational model. The corresponding residual stress and warpage distributions are shown in Figure 3.

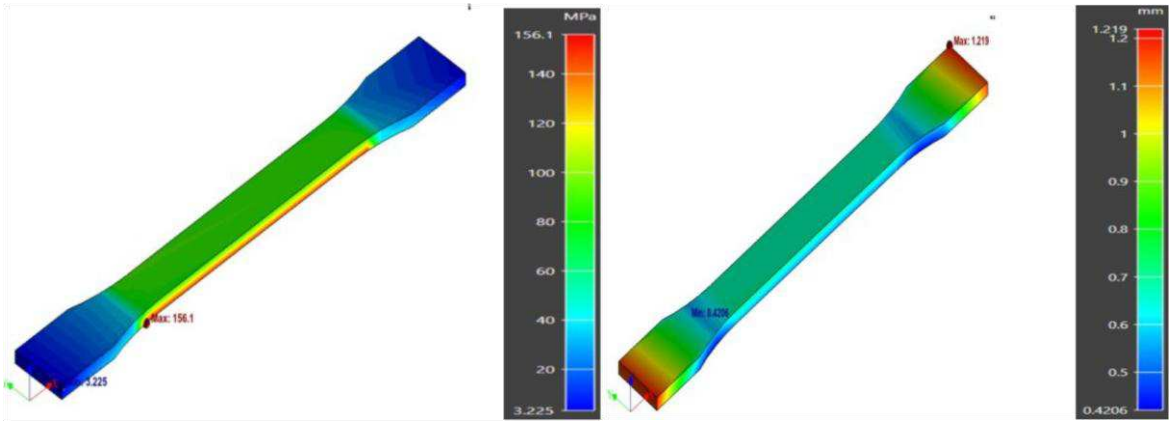

(a) (b)

Figure 3: Simulation result for extrusion temperature of 430°C, print speed of 40 mm/s, layer thickness of 0.15 mm, and chamber temperature of 120°C: (a) Residual Stress (b) Warpage

2.6 Mesh Sensitivity Analysis and Literature-based Model Assessment

The effect of finite element discretization on the predicted mechanical response of the ASTM D638 Type I tensile specimens was investigated with a mesh sensitivity study in ANSYS Workbench. For each material model, aluminium and carbon-fiber-reinforced polyetherketoneketone (CF-PEKK), separate finite element models were developed to independently study the sensitivity of the mesh. The global element size was varied in the range of 0.5 to 5 mm, and successive mesh refinements were assessed to evaluate the convergence of the predicted mechanical response. Particular attention was given to the variation in equivalent stress as the element size decreased.

Figure 4 shows the finite element mesh generated for the tensile specimen, while Figure 5 presents the corresponding mesh sensitivity analysis for CF-PEKK and aluminium. Predicted equivalent stress values were sensitive to mesh refinement until convergence. For element sizes greater than 1.5 mm, the predicted stress results were essentially the same, indicating that further mesh refinement did not significantly change the calculated stress response. Therefore, an element size of 1.0 mm was selected for the following comparative tensile simulations. This selection provided a suitable balance between computational cost and numerical accuracy while reducing the influence of mesh discretization on the predicted mechanical response. Assessing mesh sensitivity is particularly important in numerical simulations involving composite materials, where appropriate spatial discretization is necessary to obtain consistent predictions of stress, strain and deformation [29].

The numerical predictions were compared with experimental findings reported in the literature for additively manufactured polyaryletherketone (PAEK)-based materials. This literature-based comparison was used to examine the consistency of the predicted mechanical behaviour with

previously reported findings. Differences in material composition, manufacturing conditions and experimental configurations were considered when interpreting the comparisons. The comparison therefore provides a literature-based assessment of the predicted response rather than direct experimental validation of the present numerical models.

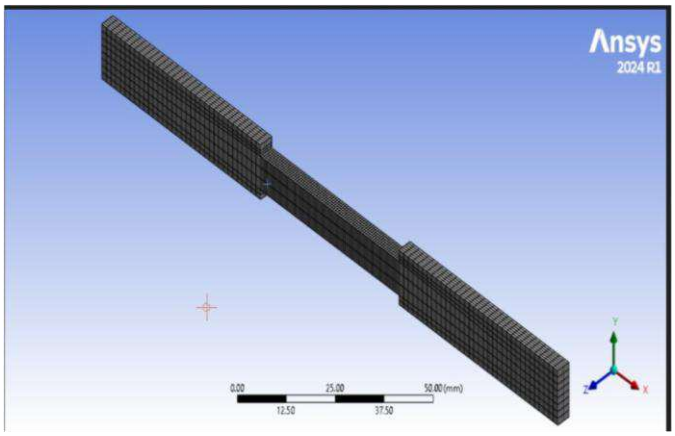

Figure 4: Meshed Tensile Specimen

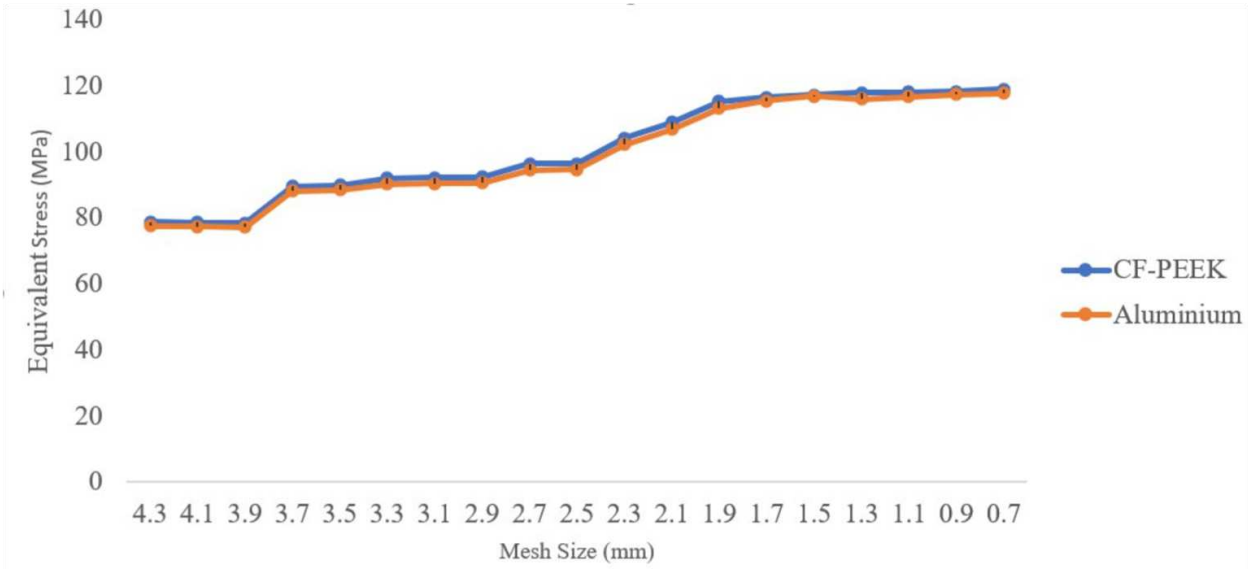

Figure 5: Mesh sensitivity analysis showing equivalent stress as a function of mesh size for CF-PEKK and Aluminium

2.7 Taguchi Design of Experiments

The effect of the FFF processing parameters on the predicted thermo-mechanical responses of the CF-PEKK was investigated through the Taguchi design of experiments (DOE) method. Minitab was used to generate a Taguchi L9 orthogonal array to minimize the number of simulation combinations required for the estimation of the selected process parameters.

Four process parameters were considered: chamber temperature, extrusion temperature, print speed and layer thickness. All factors were considered at three levels, leading to nine simulation combinations using the orthogonal array L9. Process parameters and their levels are shown in Table 2.

Table 2. Process parameters and levels used in the Taguchi L9 design

Process parameter	Level 1	Level 2	Level 3
Chamber temperature (°C)	120	140	160
Extrusion temperature (°C)	380	400	430
Printing speed (mm/s)	15	25	40
Layer thickness (mm)	0.10	0.15	0.25

The G-code files for the selected printing parameters were generated using Creatware slicing software and used in DIGIMAT-AM for the deposition-process simulations. The numerical results obtained were analyzed to study the effect of the selected manufacturing parameters on the residual stress and warpage.

The simulation outputs were then analyzed to identify the relative influence of the investigated process parameters and to determine the parameter combination associated with the preferred thermo-mechanical response. The analysis involved the evaluation of the stress fields and displacement and the relevant stress components ($\sigma 11$, $\sigma 12$, $\sigma 22$, $\sigma 33$).

The warpage response was assessed from the displacement field, considering only the out-of-plane deformation in relation to the original build geometry. The resultant residual stress and warping predictions were considered the major responses to evaluate the effect of the FFF process parameters.

Based on the available literature, four process parameters were selected for the present investigation: nozzle (extrusion) temperature, chamber temperature, printing speed and layer thickness. These parameters were selected because of their reported influence on the thermal and mechanical behaviour of PAEK-based materials, as summarized in Table 3.

Table 3 shows that the four selected parameters were therefore considered appropriate for evaluating their effects on the predicted residual stress and warpage of FFF-processed CF-PEKK. Their influence was investigated using an L9 Taguchi orthogonal array, with the parameter levels defined in the experimental design presented in the following subsection.

Table 3: Experimental evidence supporting the selected process parameters

Study	Material	Nozzle temperature	Chamber temperature	Printing speed	Layer thickness	Other parameters	Main response
Rabinowitz et al. [18]	CFR-PEKK	Investigated	Not reported	Investigated	Investigated	Nozzle diameter, rester angle	Flexural strength
Maloney et al. [24]	PEKK	Investigated	Not reported	Investigated	Investigated	Build-platform temperature	Flexural, physical and thermal properties
Tetteh et al. [56]	PEKK/PEEK	Investigated	Investigated	Investigated	Investigated	Microscopy, DSC	Compressive modulus, yield strength
Malekpour and Hojjati [57]	PEKK	Fixed	Fixed	Fixed	Fixed	Build orientation	Tensile and flexural properties
Rashed et al. [58]	PAEK-based composite	Not reported	Not reported	Not reported	Not reported	Orientation, infill, contours, raster angle	Tensile properties
Maloney et al. [59]	PEKK	Fixed	Fixed	Fixed	Fixed	Annealing temperature	Tensile/flexural properties, crystallinity
Premanand et al. [60]	PAEK-based material	Not reported	Not reported	Not reported	Not reported	Cyclic loading/frequency	Fatigue strength
Triminì et al. [61]	PEEK	Investigated	Investigated	Investigated	Not reported	Thermal processing conditions	Crystallinity and tensile properties

3.0 Results and Discussion

3.1 Mechanical response of CF-PEKK and Aluminium

The predicted mechanical behaviours of CF-PEKK and aluminium under the applied loading conditions are compared in Table 4. The maximum equivalent von Mises stress was 118.15 MPa and 117.73 MPa, respectively; the difference is about 0.36%. This shows that the two material models have a similar stress response under the same loading and boundary conditions. However, CF-PEKK had a maximum total deformation of 0.8965 mm, whereas aluminium had a maximum total deformation of 0.15368 mm, which is about 483.0% higher. In contrast, the strain energy predicted for CF-PEKK was 0.10329 mJ and for aluminium was 0.12518 mJ, which was approximately a 17.5% reduction. The mechanical behavior of 3D printed CF-PEKK composites has been studied under different loading conditions. Nachtane et al. [42] showed that the material is very sensitive to dynamic compressive loading, which suggests the need for a more comprehensive characterization of the mechanical behaviour for different loading regimes, including the tensile loading studied in this work.

The differences in the predicted mechanical responses are due to the different material characteristics of CF-PEKK and aluminium. In particular, the orthotropic behaviour of CF-PEKK, which is due to its fiber-reinforced structure, influences the stiffness and deformation response to applied loading. Thus, the results allow a comparison of the mechanical behaviour of the two materials under the given loading conditions and not a proof of the overall mechanical superiority of CF-PEKK versus aluminium.

Table 4: Comparison of Stress, Deformation, and Strain Energy for CF-PEKK and Aluminium

Material	Maximum stress (MPa)	Maximum deformation (mm)	Strain energy (mJ)
CF-PEKK	118.15	0.8965	0.10329
Aluminium	117.73	0.15368	0.12518

3.2 Evaluation of Deformation, Residual Stress, and Warpage

Figure 6 presents the total deformation distribution of the CF-PEKK tensile specimen under the applied load predicted by DIGIMAT AM. The region of maximum deformation is 0.8965 mm, which is the region of maximum displacement of the specimen under the given loading condition.

The distribution of deformation shows the displacement response and the performance of the CF-PEKK material as a structure under the mechanical loading.

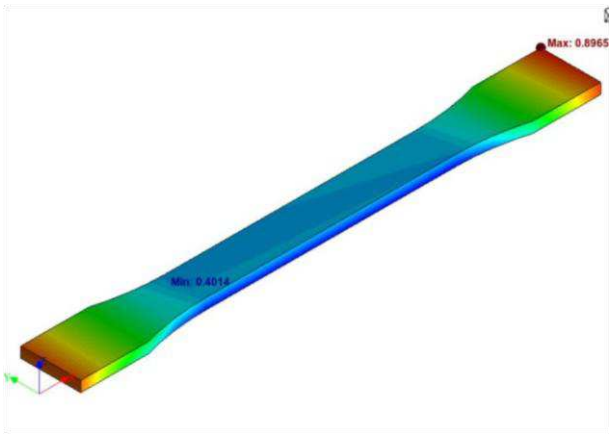

Figure 6: Total deformation distribution of the CF-PEKK tensile specimen under applied loading

Figure 7 shows the residual stress distribution predicted by the DIGIMAT AM thermomechanical simulation after the FFF process and cooling. The maximum residual stress concentration in the tensile specimen gauge section is 155.8 MPa. The results show the significance of process-induced stresses in the structural integrity assessment of additively manufactured CF-PEKK components. This comparison does not prove that yielding or failure will occur without external loading even when the predicted maximum residual stress is greater than the reported tensile strength of CF-PEKK (110 MPa). Therefore, it is necessary to consider the residual stress components, their distribution, the material's relevant strength properties, and a suitable failure criterion. However, the magnitude and location of the expected stresses suggest that residual stress has to be considered for the reliability assessment of printed parts such as the proposed motor housing.

Residual stresses are caused by non-uniform temperature gradients in processing and the subsequent cooling. Differential cooling rates across the specimen result in differential thermal contraction, which may cause internal stresses if the material is constrained. The lower layers, in particular, are limited in their ability to contract freely during cooling, as they are adhered to the heated build plate [47]. Thermal contraction of further deposited layers, which cool down, affects the development of tensile stresses in the constrained lower regions. The effect could be more evident near specimen edges due to increased exposure to the environment, causing faster heat dissipation and higher local thermal gradients [25, 45, 46].

These observations are in agreement with the results of Li et al. [35, 36], who reported an increase in tensile stresses in the gauge region during the cooling process. The results suggest that thermal

history, cooling conditions and geometrical characteristics of the printed specimen are important factors controlling residual stress distribution in FFF-processed CF-PEKK. Therefore, controlling the thermal conditions during the deposition and cooling is important to mitigate the process-induced stresses and improve the structural reliability of the printed components.

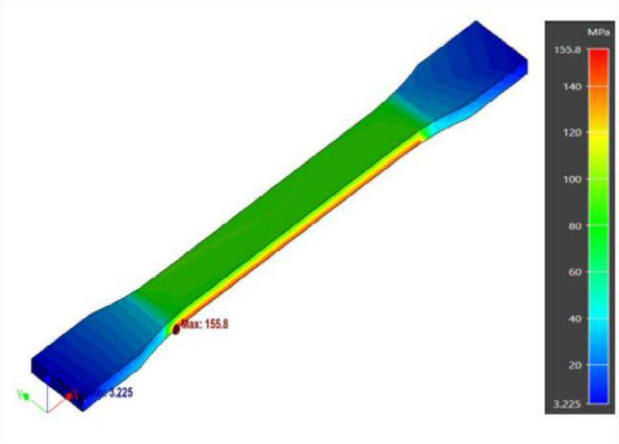

Figure 7: DIGIMAT AM simulation results showing the residual stress distribution in the CF-PEKK tensile specimen.

The directional stress components generated in the CF-PEKK specimen are presented in Figure 8. The normal stress component, σ11, in the deposition direction is presented in Fig. 8(a), and the shear stress component, σ12, is presented in Fig. 8(b). The σ11 distribution is a representation of the evolution of the normal stresses in the principal deposition direction during cooling. The concentration near the top flange suggests that geometric changes and local variations in thermal contraction influence the distribution of normal stresses in the specimen.

The σ12 distribution identifies regions of high shear stress, especially near geometric transitions and acute angles. The regions are prone to the nucleation of interlayer damage under the localized shear stresses induced by the thermal contraction and geometric constraints. This behaviour is in line with that of fiber-reinforced composites in which the stress state depends on the fiber orientation and the interaction between neighbouring deposited layers [33]. Therefore, the distributions shown in Figure 8 indicate that the geometry of the specimen and the deposition direction both influence the formation of localized stresses in the printed CF-PEKK specimen.

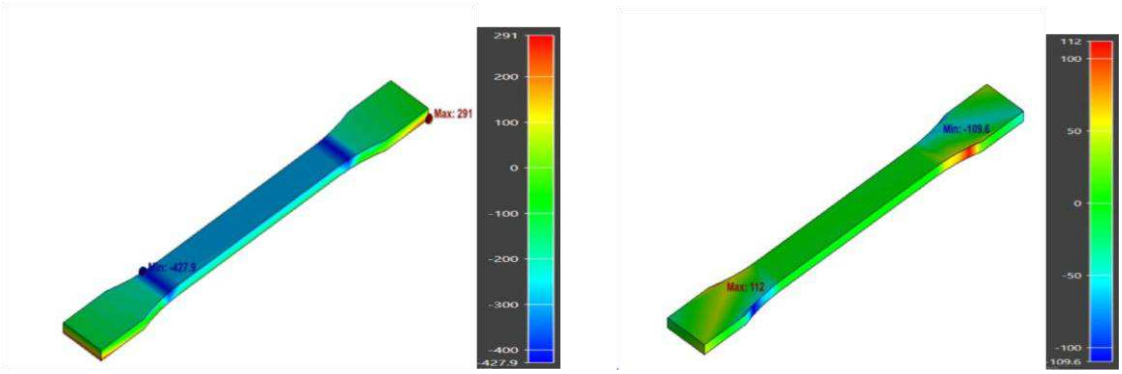

Figure 8: Stress components for CF-PEKK specimens: (a) σ11 stress components; (b) σ12 stress components

Fig. 9 shows the mean residual stress for CF-PEKK compared to results for other additively manufactured materials from the literature. The average residual stress of CF-PEKK is 150.92 MPa, which is higher than the reported value of 100 MPa for Aluminium 6061 produced by Wire Arc Additive Manufacturing (WAAM) [48, 49]. It is also higher than the reported mean residual stress of 139.87 MPa for PEEK fabricated by Fused Deposition Modelling (FDM) [51]. These results indicate that the predicted residual stress in the present CF-PEKK study is relatively high compared to the selected literature values. This discrepancy may be due to the different material systems, deposition processes, geometries, and conditions of simulation or measurement represented in the studies cited. In particular, the differences in thermal histories and material properties between FFF and WAAM may influence the levels of residual stress resulting from the process.

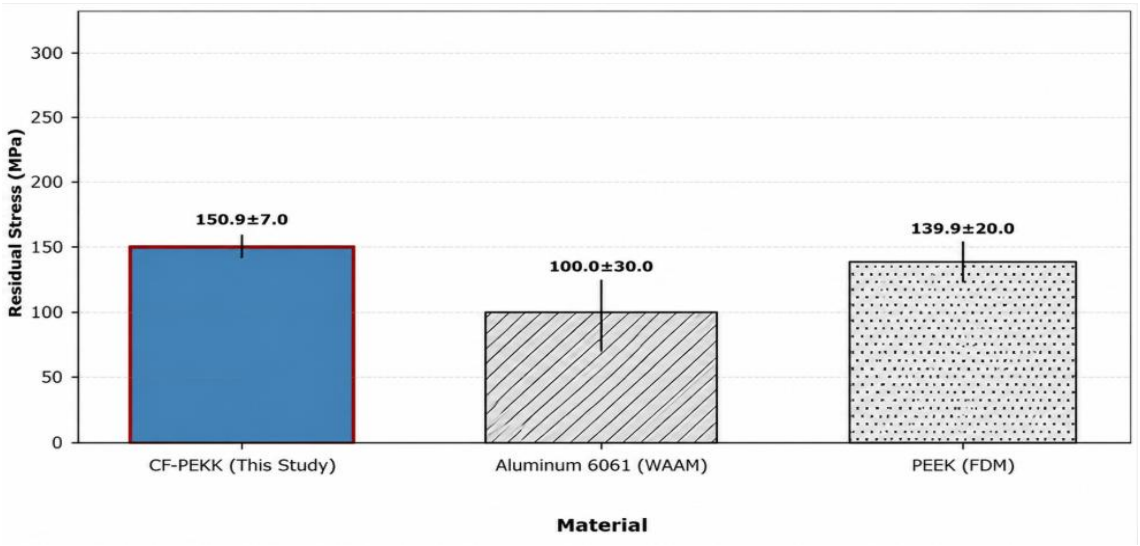

Figure 9: Residual Stress evaluation between different materials

The residual stress distributions are shown in a boxplot representation in Figure 10. The calculated residual stress values for CF-PEKK are in the range from 145.80 to 167.50 MPa, with a mean value of 150.92 MPa. The small variation observed indicates that the residual stress is not very sensitive to the combinations of parameters simulated. This suggests a fairly even distribution, with the median close to the mean. This is in comparison to the reported residual stress range of 40-100 MPa for Aluminium 6061 manufactured by WAAM [48, 49]. The reported values indicate a variation in the residual stress behaviour for the selected material and manufacturing methods.

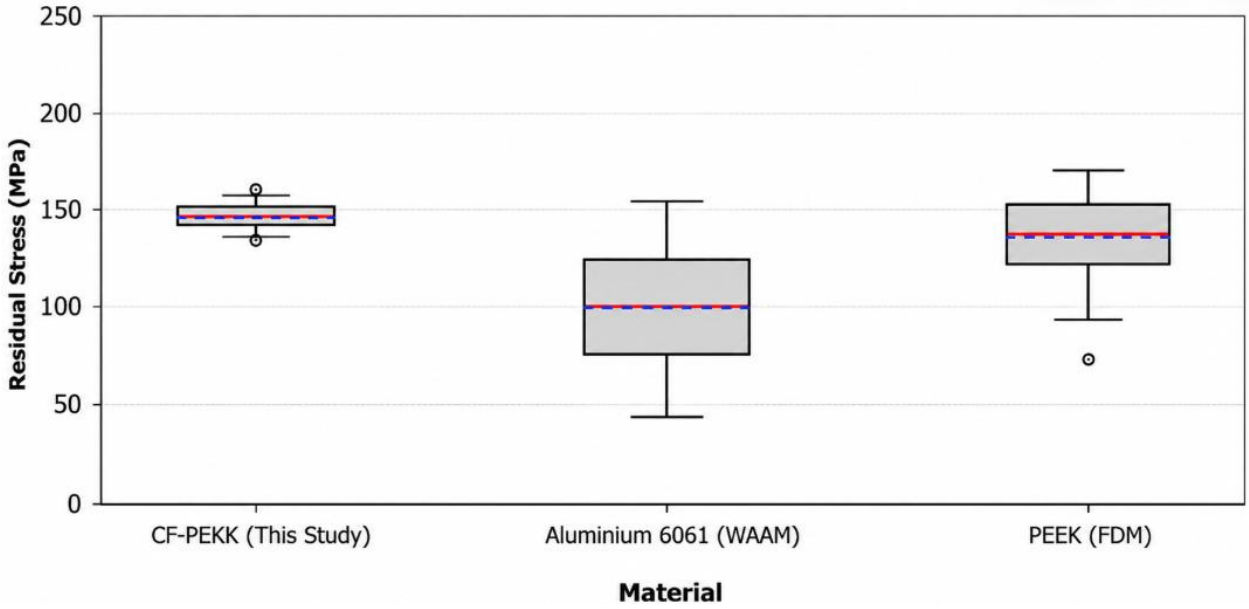

Figure 10: Comparison of Residual stress for different materials

The spatial distribution of residual stress is in agreement with those reported in earlier works. As stated by Tabatabaeian et al. [37], geometric transitions are positions for residual stresses accumulation. These localized stresses may help to initiate early fracture under subsequent mechanical loading, and thus geometric discontinuities are an important consideration when assessing the structural performance of FFF-processed components. Micromechanical and finite element simulations of fiber-reinforced polymer matrix composites were carried out by Zhao et al. [40], and they showed that residual stresses can be induced during cooling due to the differences between the thermal expansion coefficients of the matrix and reinforcement. The study reported residual stress values of approximately 140 MPa. Similarly, Zhi et al. [38] reported that residual stresses due to cooling of fiber-reinforced polymer composite parts can lead to shear stress gradients and warping, especially in the vicinity of component edges.

Figure 11 compares the warpage results of CF-PEKK, Aluminium 6061 and PEEK made by additive manufacturing processes. The mean warpage obtained for CF-PEKK is 0.966 mm, which is higher than reported values for PEEK (0.34 mm) [53] and Aluminium 6061 manufactured using WAAM (0.50 mm) [54]. Both FFF and WAAM are layer-wise manufacturing techniques, and

despite different deposition mechanisms and thermal histories, residual stress development and dimensional distortion can be attributed to the non-uniform thermal gradients and material contraction [54]. Therefore, the comparison provides a literature-based indication of the relative warpage levels and not a direct comparison under the same processing conditions.

The standard deviation of 0.185 mm obtained for CF-PEKK represents the variation of warpage across the simulated parameter combinations. The observed behaviour can be explained by several factors such as the chosen printing parameters, the geometry of the specimen and the thermal properties of the material. The use of carbon fiber reinforcement is normally associated with higher stiffness and lower thermal expansion in the fiber direction. The composite response is dependent on the direction. The alignment of fibers during FFF can lead to anisotropic thermal shrinkage and non-uniform dimensional changes. The predicted higher warpage for CF-PEKK in this study is consistent with the findings reported by Sun et al. [51] for PEEK, who attributed increased warpage for carbon-fibre-reinforced PEEK composites to anisotropic thermal shrinkage and interlayer stress concentrations due to fiber alignment during FFF.

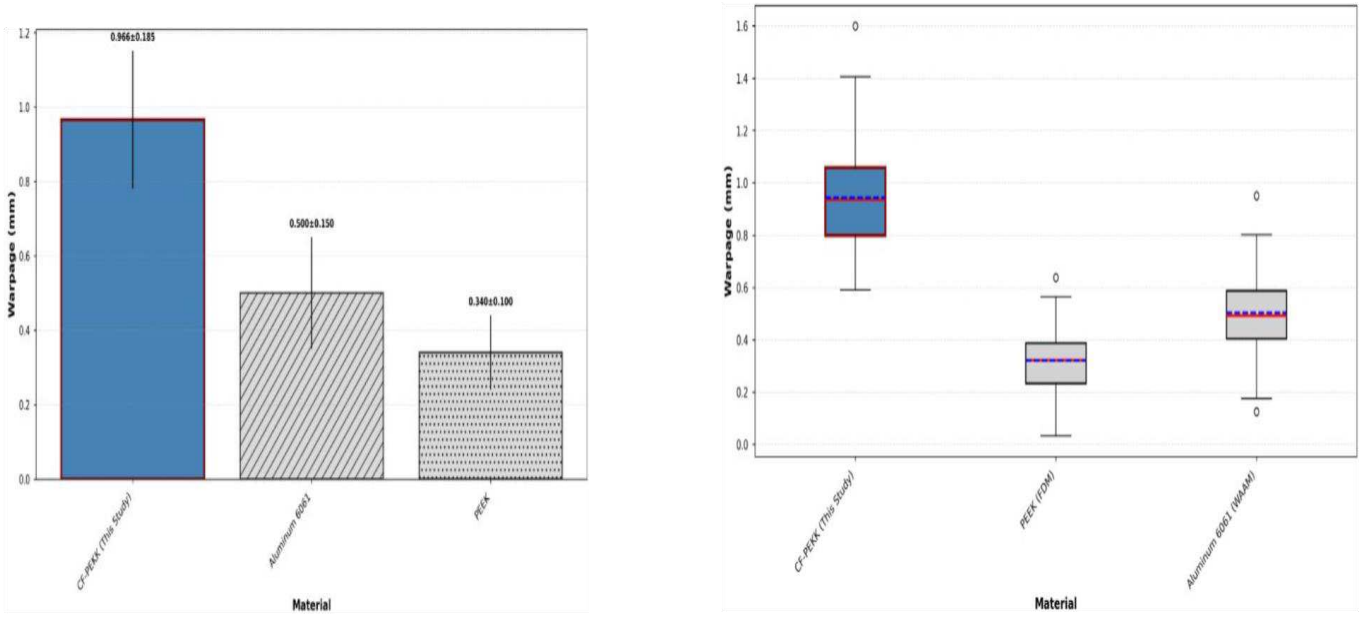

(a) (b)

Figure 11: Comparison of warpage in aluminium, CF-PEKK and PEEK (a) Graph (b) Boxplots

The graph and box plot of warpage variation for the selected material systems is shown in Fig. 11(a) and (b). The CF-PEKK results are in the range of 0.750–1.252 mm, whereas for PEEK it is 0.24–0.44 mm [53] and for Aluminium 6061 produced by WAAM it is 0.35–0.65 mm [54]. The wider range observed for CF-PEKK suggests that warpage is sensitive to the selection of process parameters. In particular, the Taguchi analysis identifies layer thickness as an important factor

influencing the predicted warpage response. This is consistent with the importance of deposition conditions and layer-wise thermal behaviour discussed in previous studies [51, 53].

Table 5 provides summary statistics that show a quantitative comparison of the results for residual stress and warpage for CF-PEKK to the literature results for Aluminium 6061 and PEEK. The CF-PEKK results, obtained from the numerical simulations conducted in the present study, give a mean residual stress of 150.92 ± 7.04 MPa and mean warpage of 0.966 ± 0.185 mm. The mean residual stress is approximately 1.5 times the reported value for Aluminium 6061 manufactured using WAAM (100 ± 30 MPa) [48, 49]. The mean warpage is approximately 2.8 times the reported PEEK value of 0.34 ± 0.10 mm [53] and 1.9 times the reported Aluminium 6061 value of 0.50 ± 0.15 mm [54]. The comparison indicates that the predicted CF-PEKK response is associated with relatively high residual stress and warpage compared with the other materials. However, the comparison is based on numerical results for CF-PEKK and published values for the other materials, rather than experimental testing under identical manufacturing conditions. The lower standard deviation of residual stress, as compared to warpage, also indicates that the predicted dimensional distortion has a larger variation over the investigated parameter combinations.

Table 5: Comparison of simulated residual stress and warpage results for CF-PEKK with values reported for other additively manufactured materials.

Material	Process	RS mean (MPa)	RS std (MPa)	RS range (MPa)	Warpage mean (mm)	Warpage std (mm)	Warpage range (mm)	References
CF-PEKK (present study)	FFF	150.92	7.04	145.8–167.5	0.966	0.185	0.750–1.252	Present study (simulation)
Aluminium 6061	WAAM	100.00	30.00	40.0–100.0	0.500	0.150	0.350–0.650	[48, 49], [54]
PEEK	FDM	139.87	20.00	120.0–160.0	0.340	0.100	0.240–0.440	[51], [53]

The predicted distributions of the directional stresses and warpage results show that the DIGIMAT AM model can capture the key thermomechanical responses of CF-PEKK during additive manufacturing. The results demonstrate the effect of thermal gradients, cooling conditions, geometrical features, and fiber orientation on the development of residual stresses and dimensional distortion. Specifically, heat dissipation control and consideration of fiber orientation in the vicinity of free edges are key to reducing process-induced stresses and warpage in FFF-processed CF-PEKK components.

3.3 Comparison of Tensile Stress Response

The predicted equivalent stress for CF-PEKK under tensile loading in the present study was 118.15 MPa, as reported in Table 4. The value was compared with numerical and experimental results available in the literature for CF-PEKK to study the agreement of the predicted mechanical response with previous literature. The predicted equivalent stress falls in the range of 113–129.6 MPa reported by Yildirim et al. [11] as shown in Table 6, while Li et al. [41] reported a stress value of approximately 200 MPa under their investigated tensile loading conditions.

The differences between the reported values may be associated with variations in specimen configuration, fiber orientation, processing conditions, loading conditions and modelling assumptions. In particular, Yildirim et al. [11] associated edge splitting in unidirectional CF-PEKK laminates with fiber misalignment. In the present study, the numerical stress distribution also indicates localized stress concentrations near the specimen edges. Although the specific mechanisms may differ between the investigated configurations, these observations highlight the importance of fiber alignment and local stress distribution in determining the tensile response of CF-PEKK components. The comparison provides a literature-based assessment of the predicted stress response rather than direct experimental validation of the present numerical model.

Table 6: Comparison of predicted tensile stress response with values reported in the literature.

Study	Material	Loading condition	Reported von Mises stress (MPa)	Key findings
Present study	CF-PEKK	Tensile loading	~120	Localised stress concentrations near specimen edges
Li et al. [36]	CF-PEKK	Tensile loading	200	Reported tensile stress response under the investigated loading conditions
Yildirim et al. [11]	CF-PEKK	Tensile loading	113–129.6	Edge splitting associated with fibre misalignment in unidirectional laminates

3.4 Effect of FFF Process Parameters on Residual Stress and Warpage

The influence of extrusion temperature, chamber temperature, printing speed and layer thickness on the predicted residual stress and warpage of CF-PEKK was investigated using an L9 Taguchi orthogonal array. The results for the nine simulation runs are presented in Table 8. The residual stress was in the range of 145.8–167.5 MPa and the warpage was in the range of 0.7496–1.2520 mm. The lowest residual stress (145.8 MPa) was obtained in Run 8, and the lowest warpage (0.7496 mm) was obtained in Run 3. In contrast, Run 2 produced the highest residual stress of 167.5 MPa, while Run 6 produced the highest warpage of 1.2520 mm. The results show that minimizing residual stress does not always minimize warpage.

Table 8. L9 Taguchi orthogonal array results for the simulated CF-PEKK specimens.

Run	Extrusion temperature (°C)	Chamber temperature (°C)	Printing speed (mm/s)	Layer thickness (mm)	Residual stress (MPa)	Warpage (mm)
1	380	120	15	0.10	147.7	0.8965
2	380	140	25	0.15	167.5	1.1770
3	380	160	40	0.25	146.5	0.7496
4	400	120	25	0.25	146.1	0.8045
5	400	140	40	0.10	146.5	0.8999
6	400	160	15	0.15	155.8	1.2520
7	430	120	40	0.15	156.1	1.2190
8	430	140	15	0.25	145.8	0.7907
9	430	160	25	0.10	146.3	0.9044

Figure 12 shows the scatter plot of the individual runs of the Taguchi DOE for CF-PEKK. The results for residual stress indicate a mean of 150.92 MPa with a large variation throughout parameter combinations. The results for warpage indicate a mean of 0.966 mm and a standard deviation of 0.185 mm. These results verify that process parameters are of significant importance for the residual stress accumulation and dimensional distortion of the CF-PEKK parts. Residual stress levels in CF-PEKK are lower than literature values for Aluminum 6061 WAAM [48, 49]

and Stainless Steel 316L LPBF [50, 52], and similar to PEEK [51]. The values of warpage are higher than those reported for PEEK [53] and Aluminum [54].

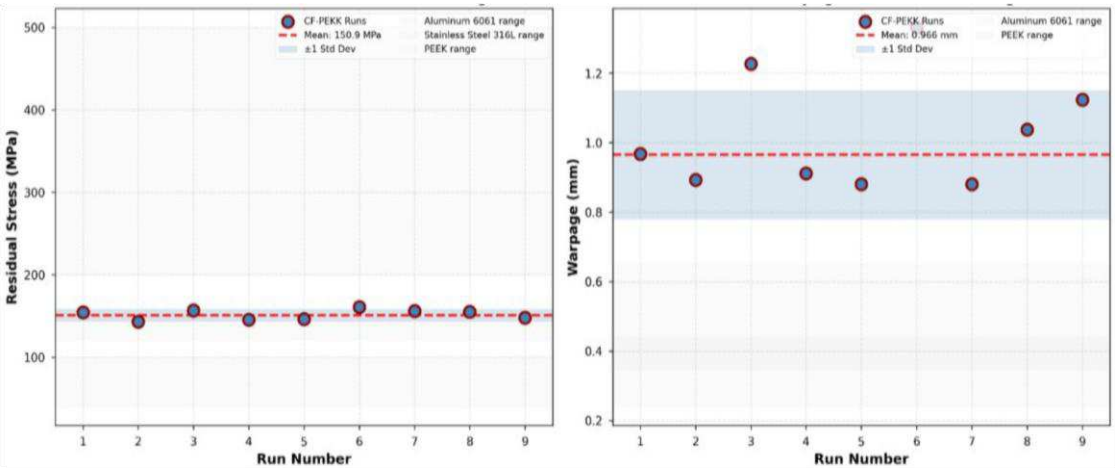

Figure 12 (a) and (b): Scatter Plots for CF-PEKK and other literature ranges

The main effects of the process parameters on the residual stress are shown in Fig. 13. The layer thickness was the most significant factor; the average residual stress increased from 146.8 MPa at 0.10 mm to 159.8 MPa at 0.15 mm and decreased to 146.1 MPa at 0.25 mm. This non-linear response indicates that the effect of layer thickness cannot be described in a simple increasing or decreasing trend. The intermediate thickness resulted in the highest mean residual stress, indicating that the changes in the deposited layer geometry and thermal history can affect the stress build-up in the printed structure.

The extrusion temperature reduced the average residual stress from 153.9 MPa at 380 °C to 149.4 MPa at 430 °C. This trend is in agreement with the potential for enhanced polymer chain mobility and better interlayer diffusion at elevated extrusion temperatures [41, 65, 66]. The chamber temperature showed non-monotonic behaviour, with the average residual stress being the highest at 140 °C (153.3 MPa) and the lowest at 160 °C (149.5 MPa). This behaviour may be related to changes in thermal gradient during deposition and cooling. The effect of printing speed on average residual stress was negligible in the range studied, from 149.7 to 153.3 MPa. The small variation indicates that its effect on residual stress was smaller than that of the layer thickness in the selected parameter range.

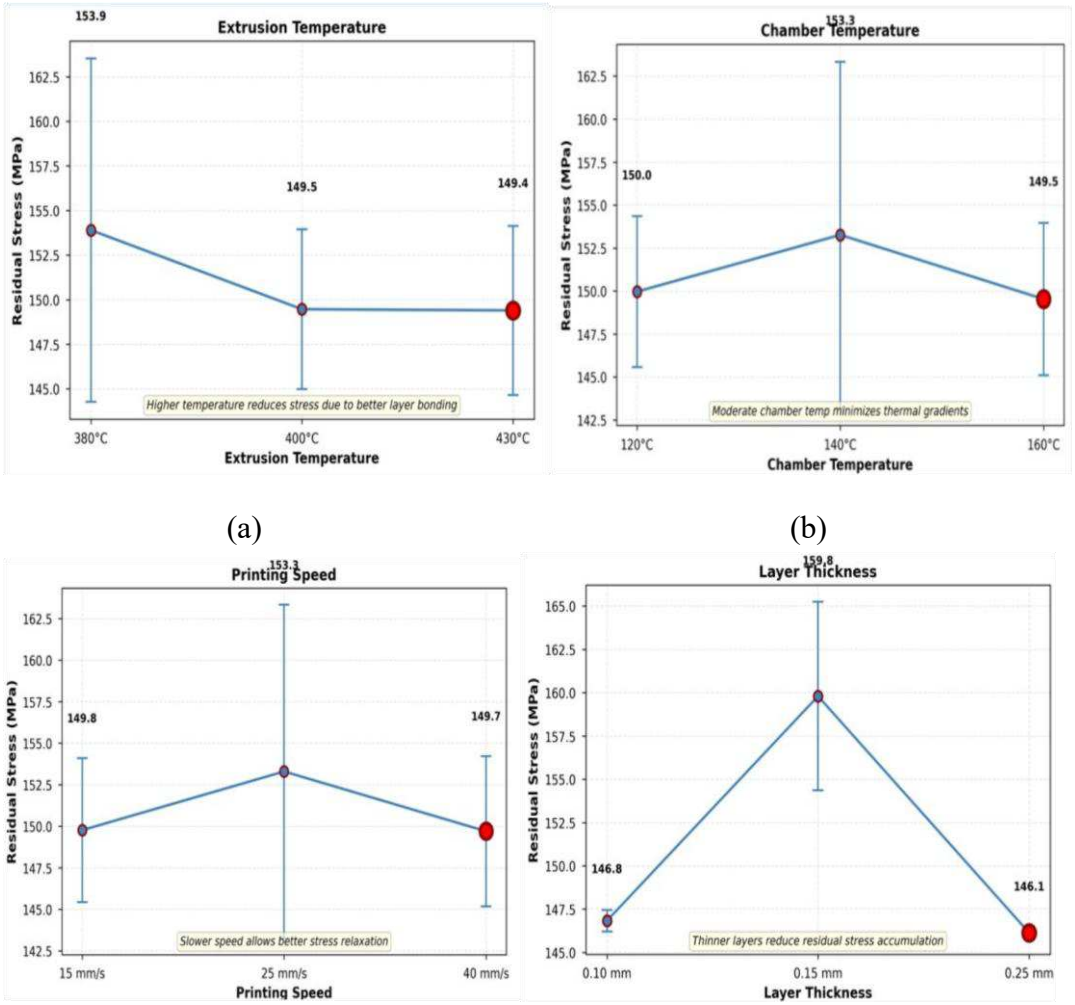

Figure 13. Main-effects plots showing the influence of (a) extrusion temperature, (b) chamber temperature, (c) printing speed and (d) layer thickness on predicted residual stress.

The corresponding effects on warpage are presented in Figure 14. Layer thickness also has the highest influence, with the average warpage reducing from 0.900 mm at 0.10 mm to 0.782 mm at 0.25 mm. However, for an intermediate layer thickness of 0.15 mm, the average warpage was much higher, 1.216 mm. This response is consistent with the non-linear trend observed for residual stress and indicates that the intermediate layer thickness was less favourable for dimensional stability under the simulated conditions.

The average warpage associated with extrusion temperature varied only slightly, from 0.941 mm at 380 °C to 0.985 mm at 400 °C, before decreasing to 0.971 mm at 430 °C. The chamber temperature produced a minimum average warpage of 0.956 mm at 140 °C, compared with 0.973 mm at 120 °C and 0.969 mm at 160 °C. Increasing printing speed from 15 to 40 mm/s was associated with a gradual reduction in average warpage from 0.980 to 0.956 mm. These variations

indicate that extrusion temperature, chamber temperature and printing speed had comparatively smaller effects on warpage than layer thickness within the investigated ranges.

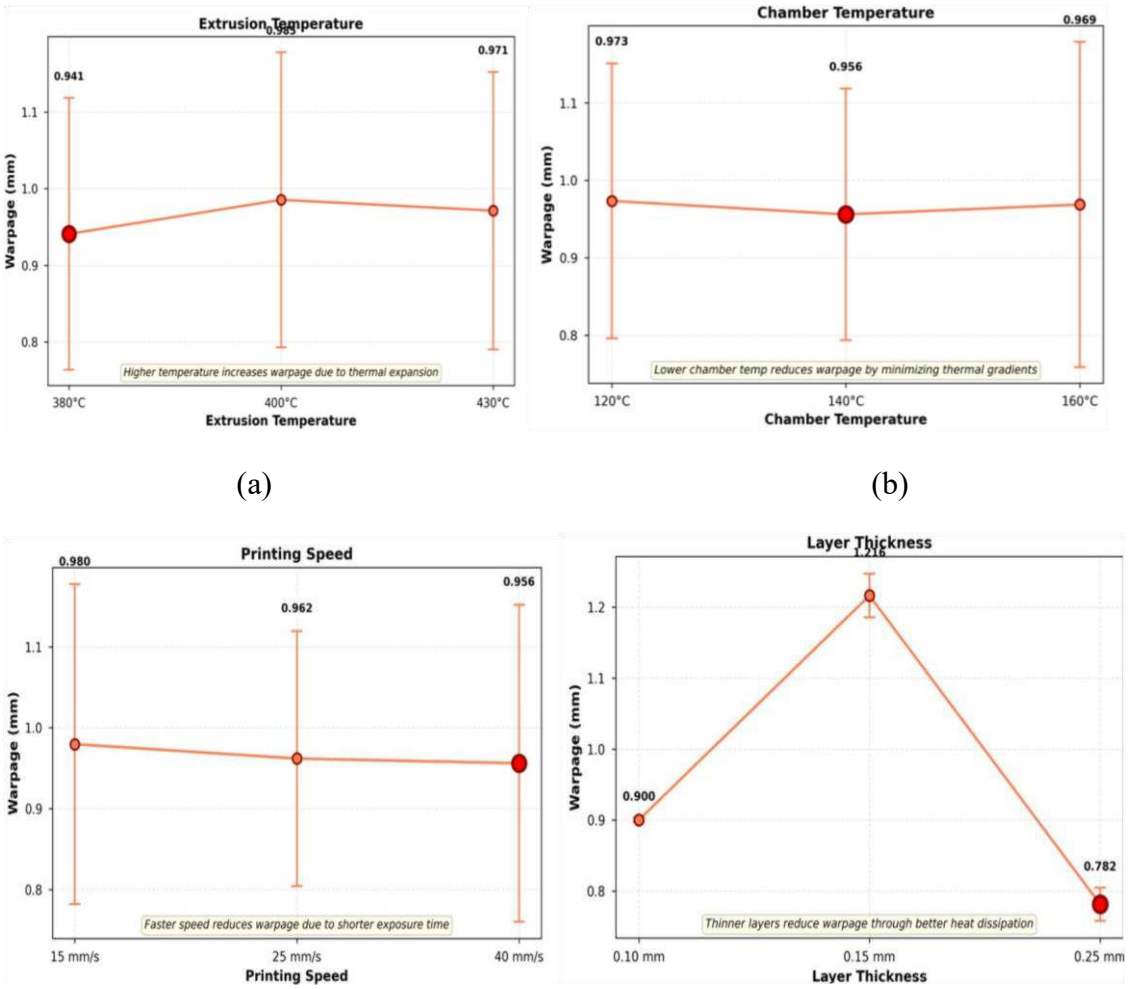

Figure 14. Main-effects plots showing the influence of (a) extrusion temperature, (b) chamber temperature, (c) printing speed, and (d) layer thickness on predicted warpage.

The signal-to-noise (S/N) response analysis for residual stress is presented in Table 9. The smaller-is-better criterion was adopted because lower residual stress was the desired response. Layer thickness had the highest delta value (0.77), followed by extrusion temperature (0.25), chamber temperature (0.20) and printing speed (0.19). The ranking is based on the analysis of the main effects, which showed that the layer thickness is the most important factor of the four factors studied in terms of residual stress. The S/N response showed that the highest S/N values were correlated with the third level of extrusion temperature (430 °C), the third level of chamber temperature (160 °C) and the third level of layer thickness (0.25 mm). For printing speed, the first and third levels had similar S/N values; the mean-response analysis was therefore also considered when identifying the preferred level.

Table 9: S/N response table for residual stress using the smaller-is-better criterion.

Level	Extrusion temperature	Chamber temperature	Printing speed	Layer thickness
1	−40.72	−40.51	−40.49	−40.33
2	−40.48	−40.68	−40.68	−41.06
3	−40.47	−40.48	−40.49	−40.28
Delta	0.25	0.20	0.19	0.77
Rank	2	3	4	1

To avoid combining responses with different physical units, the mean-response analysis was evaluated separately for residual stress and warpage. Table 10 presents the average response at each factor level. For residual stress, the lowest level means occurred at 430 °C extrusion temperature, 160 °C chamber temperature, 40 mm/s printing speed and 0.25 mm layer thickness. For warpage, the corresponding levels were 380 °C, 140 °C, 40 mm/s and 0.25 mm, respectively. Layer thickness remained the most influential factor for both responses, although the preferred temperature settings differed.

Table 10: Mean response values for residual stress and warpage at each process-parameter level.

Process parameter	Level	Residual stress (MPa)	Warpage (mm)
Extrusion temperature	380 °C	153.90	0.941
	400 °C	149.47	0.985
	430 °C	149.40	0.971
Chamber temperature	120 °C	149.97	0.973
	140 °C	153.27	0.956
	160 °C	149.53	0.969
Printing speed	15 mm/s	149.77	0.980
	25 mm/s	153.30	0.962

	40 mm/s	149.70	0.956
Layer thickness	0.10 mm	146.83	0.900
	0.15 mm	159.80	1.216
	0.25 mm	146.13	0.782

Overall, the results demonstrate that layer thickness was the dominant parameter affecting both predicted residual stress and warpage within the investigated design space. However, the different preferred temperature settings for the two responses indicate that minimizing residual stress alone does not necessarily minimize dimensional distortion. The main-effects combinations therefore provide candidate settings for subsequent multi-response optimization rather than confirmed optimum processing conditions.

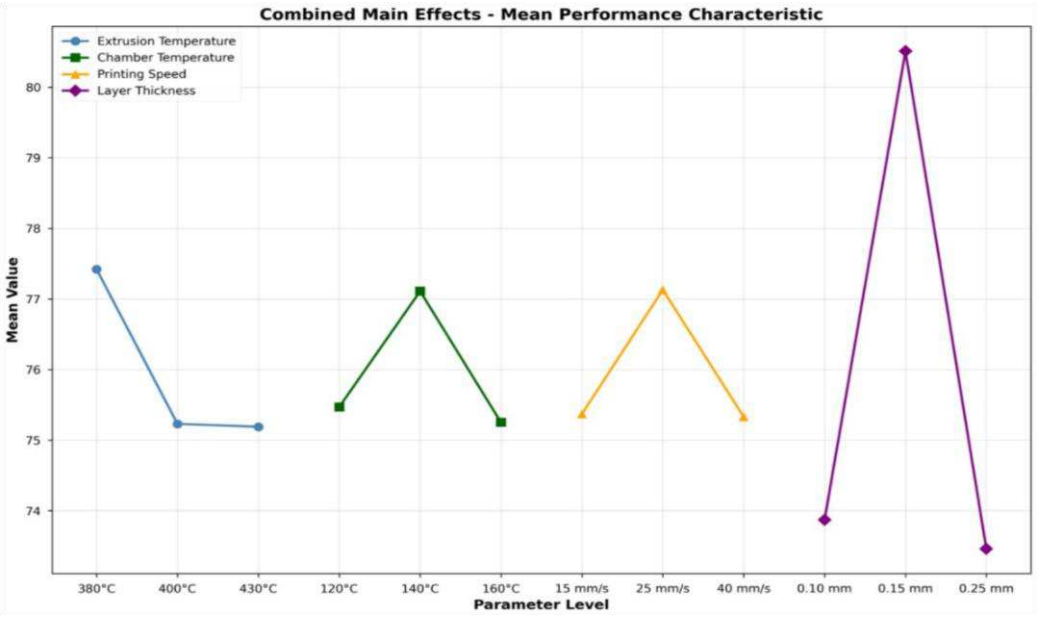

Figure 15: Main-effects plot for mean residual stress showing the influence of extrusion temperature, chamber temperature, printing speed and layer thickness.

The main-effects analysis also shows which combination of parameters leads to the lowest predicted mean residual stress. Figure 15 shows that the mean residual stress decreased from 153.90 MPa to 149.40 MPa with the increase of the extrusion temperature from 380 °C to 430 °C. The chamber temperature behaved non-linearly, with a minimum average residual stress of 149.53 MPa at 160°C. Similarly, a printing speed of 40 mm/s resulted in a lower mean residual stress than 25 mm/s, while a layer thickness of 0.25 mm resulted in the lowest mean residual stress (146.13

MPa) of the levels investigated. The increase in mean residual stress at a layer thickness of 0.15 mm also demonstrates the sensitivity of the predicted response to layer thickness.

Based on the main-effects analysis, the parameter combination of 430°C extrusion temperature, 160°C chamber temperature, 40 mm/s printing speed, and 0.25 mm layer thickness is predicted to provide the lowest mean residual stress. This combination represents a candidate processing condition derived from the Taguchi analysis and requires confirmatory simulation and experimental investigation before it can be considered an optimum processing condition. The results also reinforce the importance of layer thickness in controlling the predicted residual stress and warpage of FFF-processed CF-PEKK components [43, 44].

The optimized parameters obtained in this study are directly applicable for e-motorbike applications where CF-PEKK components can provide weight-saving, high strength solutions for battery housings, structural brackets and motor casings. The parameter optimization of e-motorbike components is especially important for the reduction of the residual stress and warpage. The components must be produced to close dimensional tolerances to guarantee proper assembly and structural integrity under dynamic loading conditions. The fabrication of low-distortion CF-PEKK parts shows good prospects for the material in weight-sensitive electric mobility applications.

3.5 Implications and Limitations

The results emphasize the significance of FFF process parameter selection for controlling the predicted residual stress and warpage of CF-PEKK components. The layer thickness was the most significant factor of the four parameters studied, and a layer thickness of 0.25 mm resulted in the lowest average warpage and residual stress for the factor levels investigated. However, it was not the same parameter combination that gave the lowest predicted residual stress and warpage for all factors. This indicates that process parameter selection requires consideration of both responses rather than relying on a single performance indicator. The Taguchi analysis therefore provides a basis for identifying promising processing conditions for further investigation, rather than establishing a universally optimal processing window.

The findings should be interpreted within the scope of the numerical framework adopted in this study. The thermomechanical behaviour associated with the FFF process, including residual stress and warpage, was simulated using DIGIMAT AM, whereas the mechanical response of the tensile specimen under applied loading was evaluated separately using ANSYS Workbench. Furthermore, comparisons with previously published studies provided a literature-based assessment of the predicted responses rather than direct experimental validation of the numerical models.

Another limitation is that the Taguchi L9 orthogonal array evaluates a selected number of parameter combinations and does not fully resolve all possible interactions among the process parameters. In addition, the numerical predictions depend on the material properties, constitutive

assumptions and process conditions defined in the respective simulation models. Experimental investigations are therefore required to validate the predicted residual stress, warpage and mechanical response of additively manufactured CF-PEKK specimens.

4.0 Conclusion

A thermo-mechanical model was developed to predict the effects of warpage and residual stress during FFF of CF-PEKK. The predicted tensile response of CF-PEKK in good agreement with experimental results presented in the literature. Thermal analysis revealed that the residual stress and warpage formation are dependent on the temperature profile occurring within the FFF process, with larger residual stresses being developed near constrained edges due to rapid cooling. The Taguchi L9 orthogonal array was employed to optimize the process parameters for minimum residual stress and warpage. The most significant parameter affecting the residual stress and warpage was the layer thickness, followed by extrusion temperature, chamber temperature and printing speed. The findings obtained from the study prove the feasibility of using CF-PEKK for e-motorbike applications. Future studies will extend the analysis to fatigue and thermomechanical performance of CF-PEKK to support application in e-mobility.

Paper Declarations

Author contributions

ADW and RN contributed to SPLRA 3D printing, code development, 3D designs, paper preparation, paper draft, and SPLRA assembly. KK and NJB contributed to supervision.

Funding

This paper was funded by The Network for Zero-defect and Zero-waste Digital Manufacturing for

Electric Vehicles Components (NeDMEV), Grant Number: 101144276

Data availability

The data generated during and/or analyzed during the current study are available from the corresponding author on reasonable request.

Ethics approval and consent to participate

Not applicable.

Consent for publication

Not Applicable

Competing interests

The authors declare no competing interests.

References

1. Larminie, J., Lowry, J. Electric Vehicle Technology Explained. *Wiley*, Chichester (2003).
2. Candela, A., Sandrini, G., Gadola, M., Chindamo, D., Magri, P. Lightweighting in the automotive industry as a measure for energy efficiency: Review of the main materials and methods. *Heliyon* 10(8), e29728 (2024). https://doi.org/10.1016/j.heliyon.2024.e29728
3. Neelakandan, V., Ganesan, T., Rao, P.C. Weight optimization of housing bracket for electrical starter motor using FEA. *Procedia Structural Integrity* 14, 345–353 (2019). https://doi.org/10.1016/j.prostr.2019.05.043
4. Shiue, N.-C., Wang, C.-N. Assessing the Impact of Electric Vehicle Development on Automotive Metal Parts.
5. Zhang, W., Xu, J. Advanced lightweight materials for automobiles: A review. *Materials Design* 226, 110994 (2022). https://doi.org/10.1016/j.matdes.2022.110994
6. Cicero, S., Lacalle, R., Cicero, R., Fernández, D., Méndez, D. Analysis of the cracking causes in an aluminium alloy bike frame. *Engineering Failure Analysis* 18(1), 36–46 (2011). https://doi.org/10.1016/j.engfailanal.2010.08.001
7. Pérez-Martín, H., Mackenzie, P., Baidak, A., Ó Brádaigh, C.M., Ray, D. Crystallinity studies of PEKK and carbon fibre/PEKK composites: A review. *Composites Part B: Applied Science and Manufacturing* 236, 109127 (2022). https://doi.org/10.1016/j.compositesb.2021.109127
8. Xin, Y.Z., Kim, D.C., Seo, J., Roh, H.D. Recent advances in manufacturing and postprocessing of fiber-reinforced thermoset and thermoplastic composites: A multi-domain perspective. *Polymer Testing* 156, 109111 (2026). https://doi.org/10.1016/j.polymertesting.2026.109111
9. Boopathi, N.G., et al. Modeling and Simulation of Electric Motors Using Lightweight Materials. *Energies* 15(14), 5183 (2022). https://doi.org/10.3390/en15145183
10. Li, X., Kumar, S., Hwang, D.W., Shin, D.H., Bae, S.Y., Kim, Y.H. Geometry and temperature effects on tensile properties and failure behaviors of open-hole and bolted-joint CF/PEKK composites. *Composites Part A: Applied Science and Manufacturing* 185, 108336 (2024). https://doi.org/10.1016/j.compositesa.2024.108336
11. Yildirim, C., Ulus, H., Sas, H.S., Topal, S., Yildiz, M. Assessing the fracture and dynamic mechanical performance of CF/PEKK joints bonded with epoxy-based adhesive film for aerospace applications: Impact of thermal and cycling hygrothermal conditions. *Composites Part A: Applied Science and Manufacturing* 190, 108659 (2025). https://doi.org/10.1016/j.compositesa.2024.108659

12. Coulson, M., Dantras, E., Olivier, P., Gleizes, N., Lacabanne, C. Thermal conductivity and diffusivity of carbon-reinforced polyetherketoneketone composites. *Journal of Applied Polymer Science* 136(38), 47975 (2019). https://doi.org/10.1002/app.47975

13. Yap, T., et al. In-plane properties of an in-situ consolidated automated fiber placement thermoplastic composite. *Composites Part A: Applied Science and Manufacturing* 188, 108525 (2025). https://doi.org/10.1016/j.compositesa.2024.108525

14. Yildirim, C., Tabrizi, I.E., Al-Nadhari, A., Topal, S., Beylergil, B., Yildiz, M. Characterizing damage evolution of CF/PEKK composites under tensile loading through multi-instrument structural health monitoring techniques. *Composites Part A: Applied Science and Manufacturing* 175, 107817 (2023). https://doi.org/10.1016/j.compositesa.2023.107817

15. Korayem, A.E., Venkatesan, K., Chen, S., Mapkar, J., Haq, M. Characterization of interlaminar properties across processing parameters of consolidation of CF/PEKK composites for benchmarking performance. *Polymer Composites* 46(7), 6714–6724 (2025).

16. Teke, I.T., Ertas, A.H. Pre-stress-integrated FEA for failure prediction in 3D-printed and injection-molded polymers. *Multidiscipline Modeling in Materials and Structures* (2025). https://doi.org/10.1108/MMMS-03-2025-0090

17. Shah, A.K., Palit, A., Williams, M.A., Wilson, P.F., Jain, A. Microstructural alteration and its impact on the effective stiffness of short carbon fiber-reinforced PLA in fused deposition modeling. *Composites Part A: Applied Science and Manufacturing* 199, 109229 (2025). https://doi.org/10.1016/j.compositesa.2025.109229

18. Hu, Y., Ladani, R.B., Brandt, M., Li, Y., Mouritz, A.P. Carbon fibre damage during 3D printing of polymer matrix laminates using the FDM process. *Materials Design* 205, 109679 (2021). https://doi.org/10.1016/j.matdes.2021.109679

19. Alramsi, R.M.A.A. Optimization of Automated Fiber/Tape Placement Technology for High-Performance Thermoplastic Composites. M.Sc. thesis, Khalifa University of Science and Technology (2024).

20. Al-Dhaheri, M.A., Irfan, M.S., Cantwell, W.J., Barsoum, I., Umer, R. Experimental investigation of warpage in thin CF/PEKK composite laminates consolidated under non-isothermal conditions. *Journal of Thermoplastic Composite Materials* 38(2), 679–703 (2025). https://doi.org/10.1177/08927057241256936

21. Belei, C., Joeressen, J., Amancio-Filho, S.T. Fused-Filament Fabrication of Short Carbon Fiber-Reinforced Polyamide: Parameter Optimization for Improved Performance under Uniaxial Tensile Loading. *Polymers* 14(7), 1292 (2022). https://doi.org/10.3390/polym14071292

22. Rashed, K., Kafi, A., Simons, R., Bateman, S. Effects of fused filament fabrication process parameters on tensile properties of polyether ketone ketone (PEKK*). International Journal of Advanced Manufacturing Technology* 122(9–10), 3607–3621 (2022). https://doi.org/10.1007/s00170-022-10134-1

23. Maloney, A., Gately, N., Devine, D.M. Effects of 3D Printing Parameters on the Flexural Properties of Semi-Crystalline PEKK. *Materials Today Communications* 42, 111152 (2025). https://doi.org/10.1016/j.mtcomm.2024.111152

24. Novascone, S.R., Spencer, B.W., Hales, J.D., Williamson, R.L. Evaluation of coupling approaches for thermomechanical simulations. *Nuclear Engineering and Design* 295, 910–921 (2015).

25. Zhang, H., Chen, Y., Song, W., Fan, C., Zheng, J.H., Shan, Z. Wide-temperature-range mechanical properties and precision prediction of additively manufactured continuous glass fiber reinforced PEEK composites. *Composites Part A: Applied Science and Manufacturing 202*, 109505 (2026). https://doi.org/10.1016/j.compositesa.2025.109505

26. Enriconi, M., Rodriguez, R., Araújo, M., Rocha, J., García-Martín, R., Ribeiro, J., Pisonero, J., Rodríguez-Martín, M. A comprehensive review of fused filament fabrication: Numerical modeling approaches and emerging trends. *Applied Sciences* 15(12), 6696 (2025). https://doi.org/10.3390/app15126696

27. Shanto, T.A. Improving Strength and Fracture Resistance in Fused Filament Fabrication Through Printhead-Integrated In-Situ Annealing. Ph.D. dissertation, University of Texas at Arlington (2026).

28. 3DXTECH. CarbonX_CF15_PEKK-A__TDS_v1. Grand Rapids, MI, USA. https://www.3dxtech.com/products/carbonx-pekk-a-cf15-1. Accessed 11 Jun 2026.

29. Donadon, C., Iannucci, L., Poole, P.T., Ferreira, A.J.M. A progressive failure model for composite laminates subjected to low-velocity impact. *Composites Part A: Applied Science and Manufacturing* 41(7), 898–909 (2010).

30. Bower, A.F. Applied Mechanics of Solids. CRC Press, Boca Raton (2009). https://doi.org/10.1201/9781439802489

31. Van de Werken, N., Tekinalp, H., Khanbolouki, P., Ozcan, S., Williams, A., Tehrani, M. Additively manufactured carbon fiber-reinforced composites: State of the art and perspective. *Additive Manufacturing* 31, 100962 (2020). https://doi.org/10.1016/j.addma.2019.100962

32. Murugan, R., Singamneni, S. Influence of process parameters on the mechanical behaviour and processing time of 3D printing. *International Journal of Modern Manufacturing Technologies* 10(1), 69–75 (2018).

33. Jiang, D., Smith, D.E. Anisotropic mechanical properties of oriented carbon fiber filled polymer composites produced with fused filament fabrication. *Additive Manufacturing* 18, 84–94 (2017). https://doi.org/10.1016/j.addma.2017.08.006

34. Downs, W.T., Baranack, G.S., Sayah, N., Ali, M., Trembly, J., Al-Majali, Y.T. Modeling the effect of 3D-printed induced defects on mechanical performance of natural carbon-enhanced polymer composite. *Journal of Thermoplastic Composite Materials* 39(6), 3090–3116 (2026). https://doi.org/10.1177/08927057251401101

35. Gouge, M., Michaleris, P. (eds.) Thermo-Mechanical Modeling of Additive Manufacturing. Butterworth-Heinemann, Oxford (2017). https://doi.org/10.1016/C2016-0-00317-0

36. Li, X., Zhang, M., Qi, J., Yang, Z., Jiao, Z. A simulation study on the effect of residual stress on the multi-layer selective laser melting processes considering solid-state phase transformation. *Materials* 15(20), 7175 (2022). https://doi.org/10.3390/ma15207175

37. Tabatabaeian, A., Ghasemi, A.R., Shokrieh, M.M., Marzbanrad, B., Baraheni, M., Fotouhi, M. Residual stress in engineering materials: A review. *Advanced Engineering Materials* 24(4), 2100786 (2022). https://doi.org/10.1002/adem.202100786

38. Zhi, J., Yang, B., Li, Y., Tay, T.E., Tan, V.B.C. Multiscale thermo-mechanical analysis of cure-induced deformation in composite laminates using Direct FE2. *Composites Part A: Applied Science and Manufacturing* 173, 107704 (2023). https://doi.org/10.1016/j.compositesa.2023.107704

39. Ramaswamy, K., Modi, V., Rao, P.S., Martin, P.P., McCarthy, C.T., O'Higgins, R.M. An investigation of the influence of matrix properties and fibre–matrix interface behaviour on the mechanical performance of carbon fibre-reinforced PEKK and PEEK composites. *Composites Part A: Applied Science and Manufacturing* 165, 107359 (2023). https://doi.org/10.1016/j.compositesa.2022.107359

40. Zhao, L.G., Warrior, N.A., Long, A.C. A micromechanical study of residual stress and its effect on transverse failure in polymer-matrix composites. *International Journal of Solids and Structures* 43(18–19), 5449–5467 (2006). https://doi.org/10.1016/j.ijsolstr.2005.08.012

41. Alzyod, H., Ficzere, P. Using numerical simulation to investigate the effect of layer thickness on residual stress and warping of specimens made of ABS. *Design of Machines and Structures* 12(1), 5–11 (2022). https://doi.org/10.32972/dms.2022.001

42. Nachtane, M., Tarfaoui, M., Ledoux, Y., Khammassi, S., Leneveu, E., Pelleter, J. Experimental investigation on the dynamic behavior of 3D printed CF-PEKK composite under cyclic uniaxial compression. *Composite Structures* 247, 112474 (2020). https://doi.org/10.1016/j.compstruct.2020.112474

43. Zhen, H., Zhao, B., Quan, L., Fu, J. Effect of 3D printing process parameters and heat treatment conditions on the mechanical properties and microstructure of PEEK parts. *Polymers* 15(9), 2209 (2023). https://doi.org/10.3390/polym15092209

44. Travieso-Rodriguez, J.A., Rerez-Mesa, R.J., Llumà, J., Traver-Ramos, O., Gomez-Gras, G., Rovira, J.J.R.R. Mechanical properties of 3D-printing polylactic acid parts subjected to bending stress and fatigue testing. *Materials* 12(23), 3859 (2019). https://doi.org/10.3390/ma12233859

45. Costa, S.F., Duarte, F.M., Covas, J.A. Thermal conditions affecting heat transfer in FDM/FFE: A contribution towards the numerical modelling of the process. *Virtual and Physical Prototyping* 10(1), 35–46 (2015).

46. Nelson, D. Experimental measurement of residual stress-induced in-plane displacements of as-machined polymer structures resultant from fused filament fabrication additive manufacturing. Ph.D. dissertation, University of California, Davis (2023).

47. Corvi, A., Collini, L., Sciancalepore, C., Lutey, A. Influence of process parameters on temperature field and residual strain in FFF-printed parts. *Journal of Mechanical Science and Technology* 37(11), 5521–5527 (2023).

48. Doumenc, G., Couturier, L., Courant, B., Paillard, P., Benoit, A., Gautron, E., Girault, B., Pirling, T., Cabeza, S., Gloaguen, D. Investigation of microstructure, hardness and residual stresses of wire and arc additive manufactured 6061 aluminium alloy. *Materialia* 25, 101520 (2022).

49. Doumenc, G., Courant, B., Couturier, L., Paillard, P., Girault, B., Pirling, T., Cabeza, S., Moya, M.-J., Gloaguen, D. Investigation of residual stresses and modeling of tensile deformation in wire-arc additive manufactured 6061 aluminum alloy: Diffraction and elastoplastic self-consistent model. *Materials Science and Engineering: A* 890, 145891 (2024).

50. Laurence, R.C., Canelo-Yubero, D.C., Faria, G.A., Staron, P., Ramadhan, R., Cabeza, S., Paecklar, A., Pirling, T., Martinez, J.M., Sánchez-Poncela, M., Blanc, R., Baustert, E., Miao, Z., Withers, P.J., Roy, M.J. Laser powder bed fusion residual stresses: Measurement agreement, machine parity, and baseplate-driven heat-treatment response of 316L stainless steel. *Materials & Design* 265, 115976 (2026).

51. Sun, Q., Shan, Z., Zhan, L., Wang, S., Liu, X., Li, Z., Wu, S. Warp deformation model of polyetheretherketone composites reinforced with carbon fibers in additive manufacturing. *Materials Research Express* 8(12), 125305 (2021).

52. Evans, A., Schröder, J., Pirling, T., Ulbricht, A., Ocaño, P.S., Bruno, G. Resolving the subsurface residual stress maximum in laser powder bed-fused 316L stainless steel by diffraction-based analysis. *JOM* 77, 9726–9737 (2025).

53. Zhang, H., Chen, C., Wang, J., Yang, Y., Jia, L., Yuan, X., Hui, J., Lv, J., Yan, Z. An investigation on thermal behavior and stress-warpage of poly-ether-ether-ketone parts by fused deposition modeling. *The International Journal of Advanced Manufacturing Technology* 143, 317–343 (2026).

54. Han, Y. A finite element study of wire arc additive manufacturing of aluminum alloy. *Applied Sciences* 14(2), 810 (2024). https://doi.org/10.3390/app14020810

55. Karthik, N., Bekinal, S.I., Powar, S., Doddamani, M.R. A comprehensive review of synthesis, characterization, and applications of additively manufactured PEKK and PEKK composites. *Polymer Composites* 47(3), 2024–2049 (2026). https://doi.org/10.1002/pc.70307

56. Tetteh, A.E., Smith, J.A., Porter, D.A., Di Prima, M.A., Kurtz, S.M. Investigating the impact of fused filament fabrication process parameters on the compressive properties of porous PEEK and PEKK biomaterials. *Journal of Biomedical Materials Research Part A* 114(3), e70053 (2026). https://doi.org/10.1002/jbm.a.70053

57. Malekpour, F., Hojjati, M. Tailoring anisotropy and mechanical performance of additively manufactured PEKK through annealing and architected design. *Journal of Science: Advanced Materials and Devices* 11(1), 101077 (2026). https://doi.org/10.1016/j.jsamd.2025.101077

58. Rashed, K., Kafi, A., Simons, R., Bateman, S. Optimization of material extrusion additive manufacturing process parameters for polyether ketone ketone (PEKK). *International Journal of Advanced Manufacturing Technology* 126(3–4),1067–1091 (2023). https://doi.org/10.1007/s00170-023-11167-w

59. Maloney, A., Manaf, E., Gately, N., Major, I., Devine, D.M. Annealing 3D printed PEKK: Investigating the impact of annealing on the mechanical, physical, and thermal properties in additively manufactured PEKK. *Materials Design* 253, 113938 (2025). https://doi.org/10.1016/j.matdes.2025.113938

60. Premanand, A., Schimmelpfeng, H., Balle, F. Comparability of fatigue strength and life estimation of a CF-PEKK composite under low and ultrasonic frequencies using time-temperature-based approaches. *Fatigue & Fracture of Engineering Materials & Structures* 48(5), 2363–2380 (2025). https://doi.org/10.1111/ffe.14608

61. Triminì, V., Varetti, S., Percoco, G., Corvaglia, S.G., Gallo, N., Scavo, I. Evaluation of the influence of process parameters on crystallinity and tensile strength of 3D printed PEEK parts. *Proceedings of the Institution of Mechanical Engineers, Part C*: *Journal of Mechanical Engineering Science* (2023). https://doi.org/10.1177/09544062231198784

62. Tetteh, A.E., Smith, J.A., Spece, H., Porter, D.A., Di Prima, M.A., Kurtz, S.M. Optimization of fused filament fabrication process parameters to improve the compressive

properties of PEEK and PEKK biomaterials. Journal of the Mechanical Behavior of Biomedical Materials 173, 107203 (2026). https://doi.org/10.1016/j.jmbbm.2025.107203

63. Megersa, G.K., Sitek, W., Nowak, A.J., Krzemiński, Ł., Kajzer, W., Niewolik, D. Impact of layer thickness on mechanical properties and surface roughness of FDM-printed carbon fiber PEEK composite. *Materials 19(9)*, 1692 (2026). https://doi.org/10.3390/ma19091692

64. Rodzeń, K., O'Donnell, E., Hasson, F., Boyd, A. Crystallization and microstructure effects on interlayer performance and ductility of polyetherketoneketone in open-chamber fused filament fabrication. *Materials Today Communications* 114253 (2025).

65. Lepoivre, A., Boyard, N., Levy, A., Sobotka, V. Methodology to assess interlayer quality in the material extrusion process: A temperature and adhesion prediction on a high performance polymer. *Additive Manufacturing* 60, 103167 (2022). https://doi.org/10.1016/j.addma.2022.103167

66. El Magri, A., Vanaei, S., Vaudreuil, S. An overview on the influence of process parameters through the characteristic of 3D-printed PEEK and PEI parts. *High Performance Polymers* 33(8), 862–880 (2021). https://doi.org/10.1177/09540083211009961

67. Rinaldi, M., Cecchini, F., Pigliari, L., Ghidini, T., Lumaca, F., Nanni, F. Additive manufacturing of polyether ether ketone (PEEK) for space applications: A nanosat polymeric structure. *Polymers 13(1),* 11 (2021). https://doi.org/10.3390/polym13010011

68. Han, J., Tong, J., Tian, X., Xia, L., Ma, D. Thermal simulation and warping deformation experimental study of PEEK in material extrusion. *Macromolecular Theory and Simulations* 30(2), 2000055 (2021).

69. Bergman, T.L., Lavine, A.S., Incropera, F.P., DeWitt, D.P. Fundamentals of Heat and Mass Transfer, 7th ed. *John Wiley & Sons, Hoboken* (2011).

70. Bathe, K.J. Finite Element Procedures. Prentice Hall, Upper Saddle River (1996).